Supporting Information

Chemisorption Manipulation by Adjusting the Carrier Concentration of the Adsorbent and Its Application to Adsorbate Identification

Gyuweon Jung[1,2‡], Kangwook Choi[1‡], Suyeon Ju[3‡], Jaehyeon Kim[1], Wonjun Shin[4], Seongi Lee[3], Gyuho Yeom[1], Ryun-Han Koo[1], Young-Chang Joo[3,5], Woo Young Choi[1], Seungwu Han[3], and Jong-Ho Lee[1,5*]

[1]Department of Electrical and Computer Engineering and Inter-university Semiconductor Research Center, Seoul National University, Seoul 08826, Republic of Korea

[2]School of Transdisciplinary Innovations, Seoul National University, Seoul 08826, Republic of Korea

[3]Department of Materials Science and Engineering and Research Institute of Advanced Materials, Seoul National University, Seoul 08826, Republic of Korea

[4] Department of Semiconductor Convergence Engineering, Sungkyunkwan University, Suwon 16419, Republic of Korea

[5]Ministry of Science and ICT, Sejong 30121, Republic of Korea

‡ G. Jung, K. Choi, and S. Ju contributed equally to this work.

* Corresponding author. Tel.: +82-2-880-1727; Fax: +82-2-882-4658.

E-mail address: jhl@snu.ac.kr (J.-H. Lee)

This file contains:

Supporting Information Figure S1-S13, Table S1, and Note S1-2

CONTENTS

Supplementary Figures

To investigate the effect of V_M modulation on the carrier concentration of the adsorbent, we additionally fabricated devices with various channel lengths (L) (Figure S2a). We then measured the resistance of these devices while varying the V_M (Figure S2b). The obtained resistance can be expressed as follows:

Supplementary Table

Supplementary Note

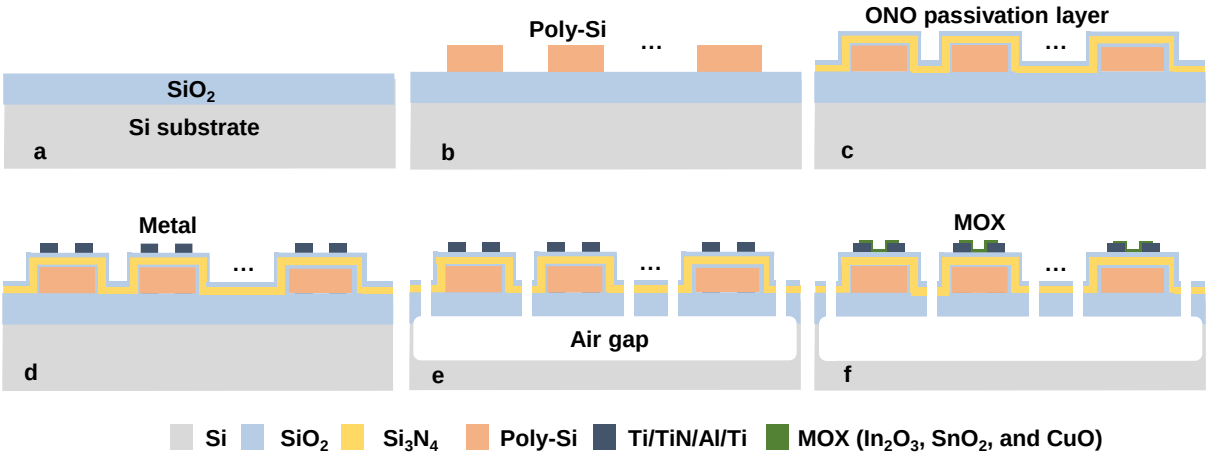

Supporting Fig. 1. Key fabrication processes of the device for manipulating chemisorption.

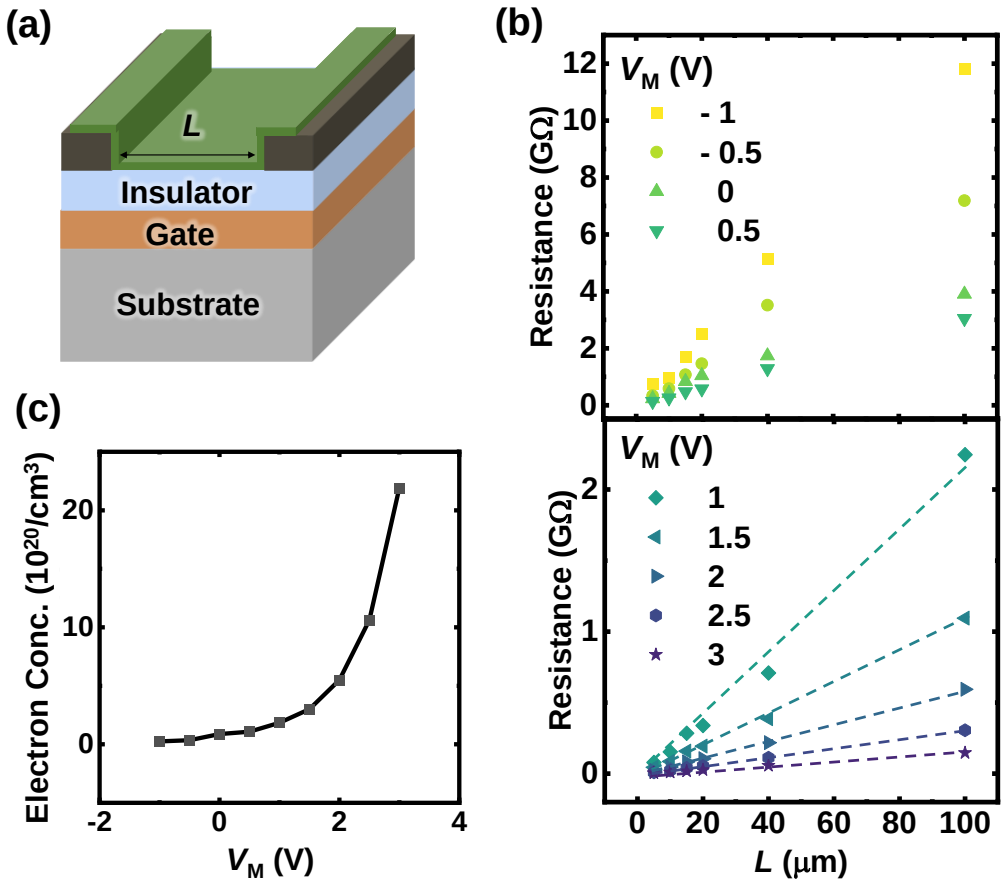

Supporting Fig. 2. (a) 3D schematic image of the device. (b) Resistance of In_2O_3 adsorbent versus channel length (L) in various V_Ms. (c) Changes in electron concentration of adsorbent depending on V_M.

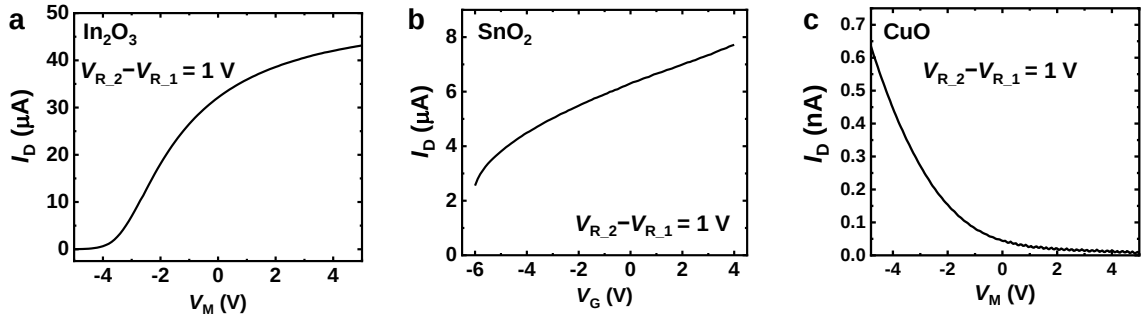

Supporting Fig. 3. Current flow (I_R) in (a) In_2O_3, (b) SnO_2, and (c) CuO adsorbents as a function of V_M.

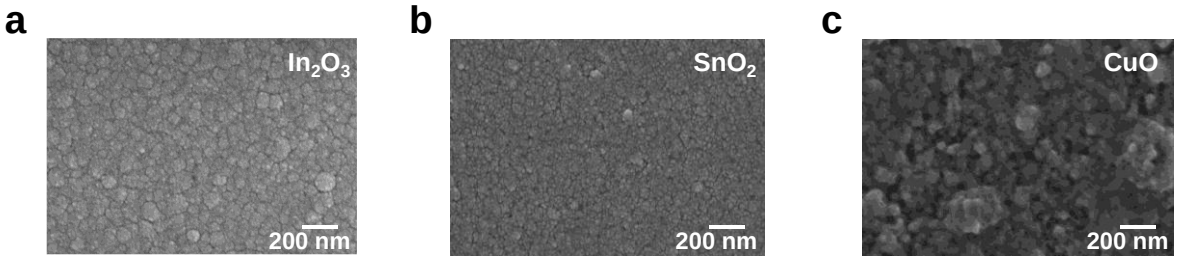

Supporting Fig. 4. Scanning electron microscope (SEM) image of (a) In_2O_3, (b) SnO_2, and (c) CuO adsorbents.

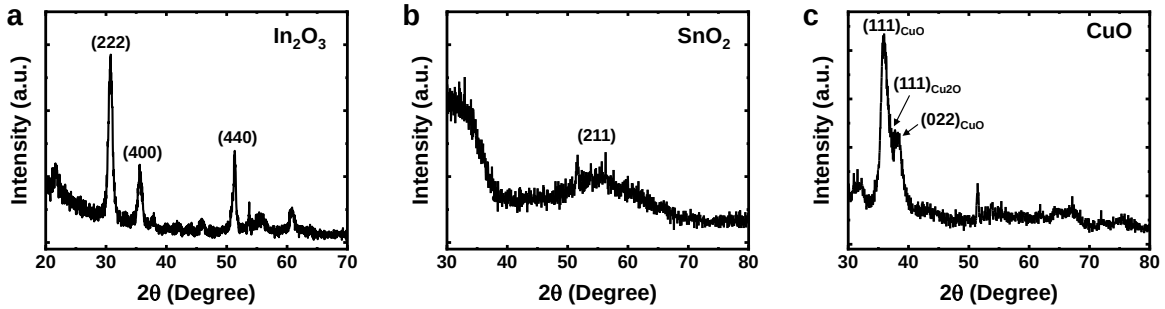

Supporting Fig. 5. Grazing incidence X-Ray diffraction (GIXRD) pattern of (a) In_2O_3, (b) SnO_2, and (c) CuO adsorbents.

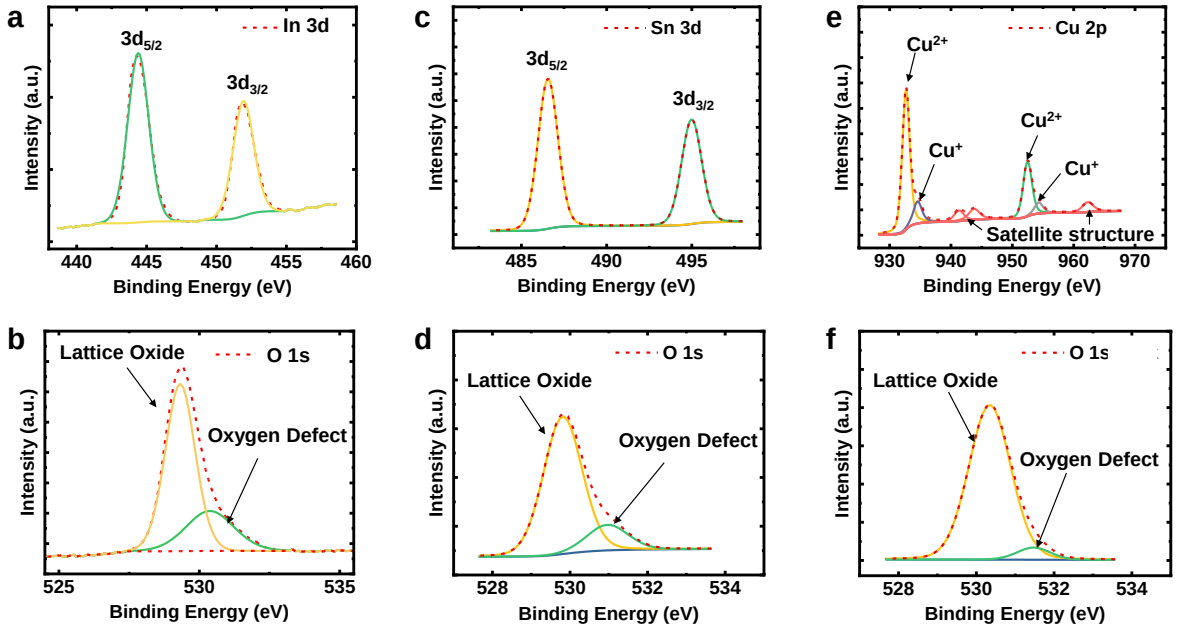

Supporting Fig. 6. High-resolution (a) In_{3d} and (b) O_{1s} core level X-ray photoelectron spectroscopy (XPS) spectra of the In_2O_3 adsorbent. High-resolution (c) Sn_{3d} and (d) O_{1s} core level XPS spectra of the SnO_2 adsorbent. High-resolution (a) Cu_{2p} and (b) O_{1s} core level XPS spectra of the CuO adsorbent.

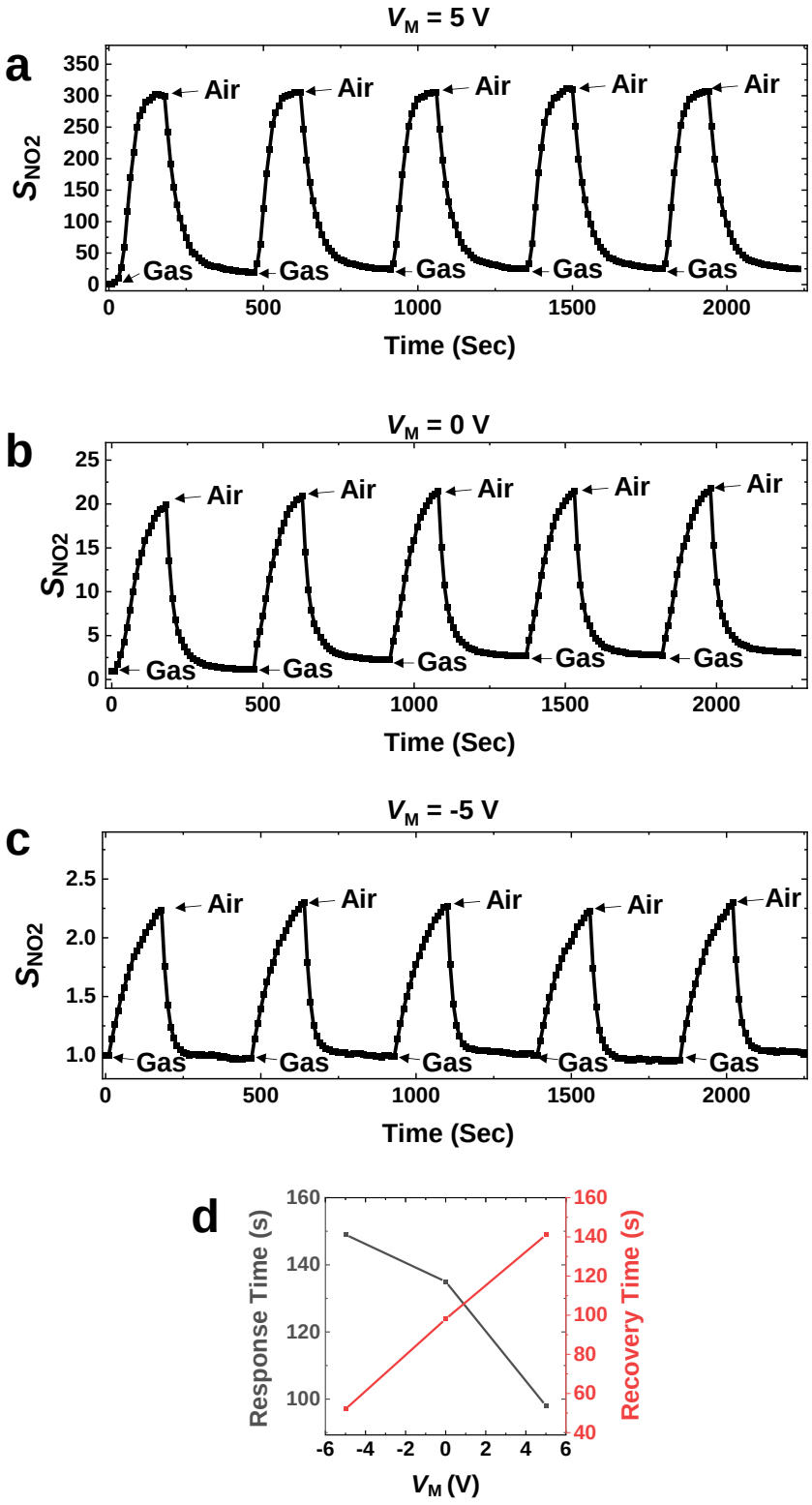

Supporting Fig. 7. Cyclic transient behavior of the device with In_2O_3 at V_M of (a) 5 V, (b) 0 V, and (c) -5 V to 500 ppb NO_2 gas. (d) Response and recovery times of the device with In_2O_3 to 500 ppb NO_2

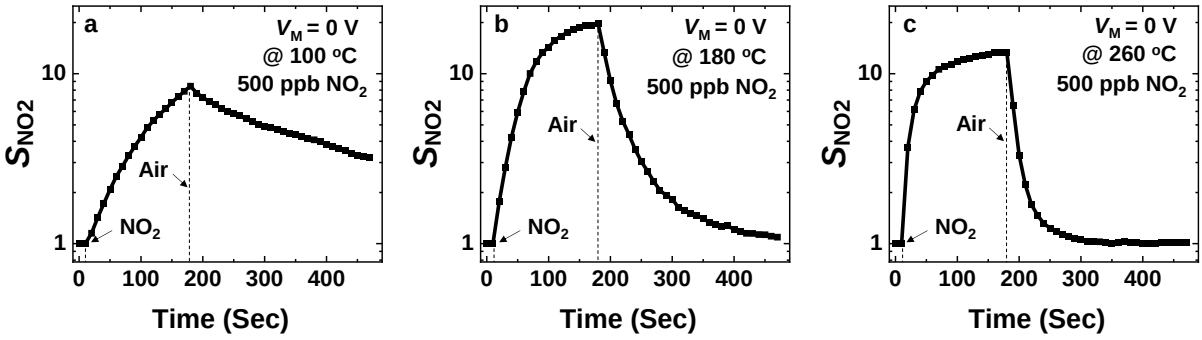

Supporting Fig. 8. Transient response behavior of the device with In_2O_3 to 500 ppb NO_2 gas at (a) 100 (b) 180, and (c) 260 °C.

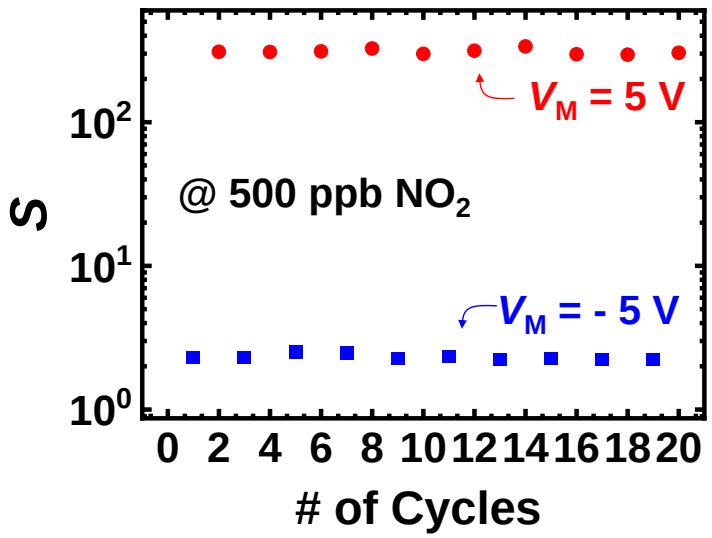

Supporting Fig. 9. Cyclic *S* behavior of the device with In_2O_3 to 500 ppb NO_2 gas.

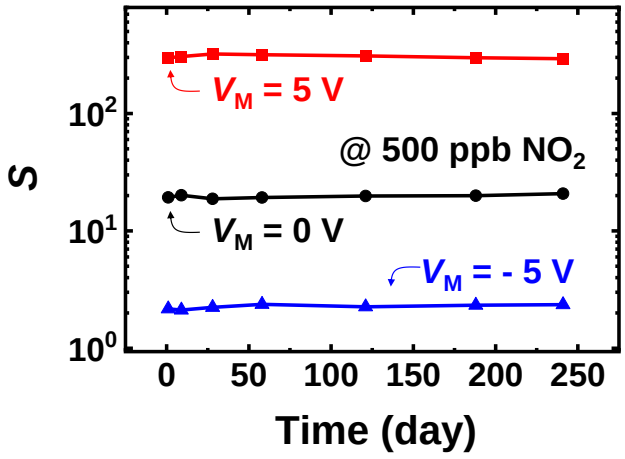

Supporting Fig. 10. Long-term stability behavior of the device with In_2O_3 to 500 ppb NO_2 gas.

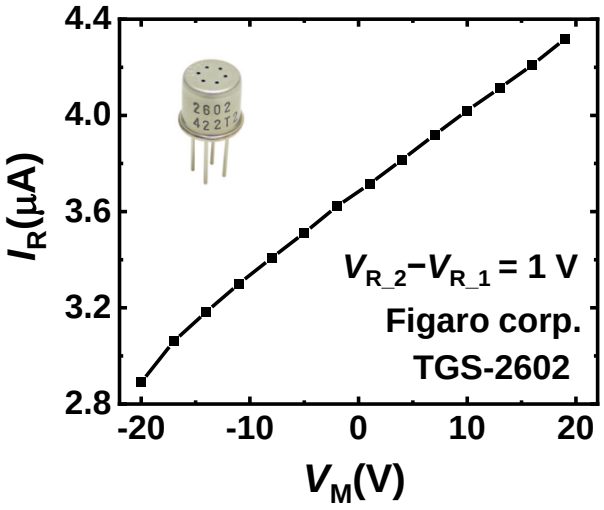

Supporting Fig. 11. I_R vs. V_M curve of TGS-2602 sensor manufactured by Figaro corporation.

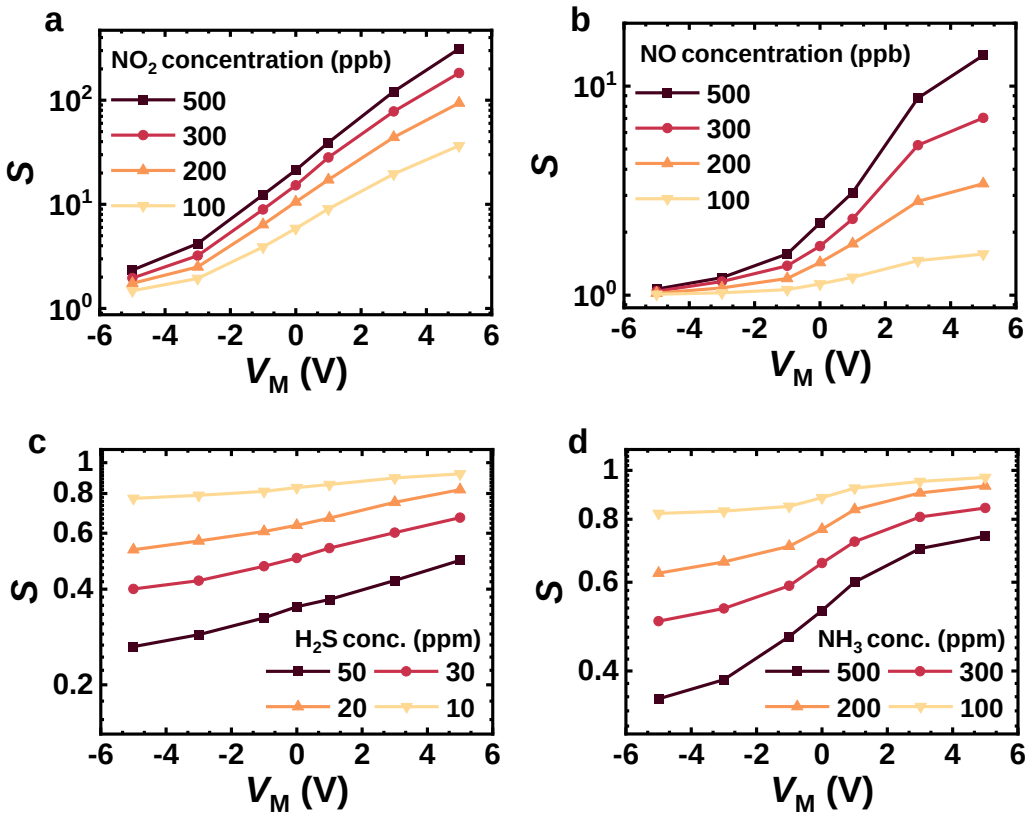

Supporting Fig. 12. S vs. V_M curves of In_2O_3 sensor for varying concentrations of (a) NO_2, (b) NO, (c) H_2S, and (d) NH_3 gases.

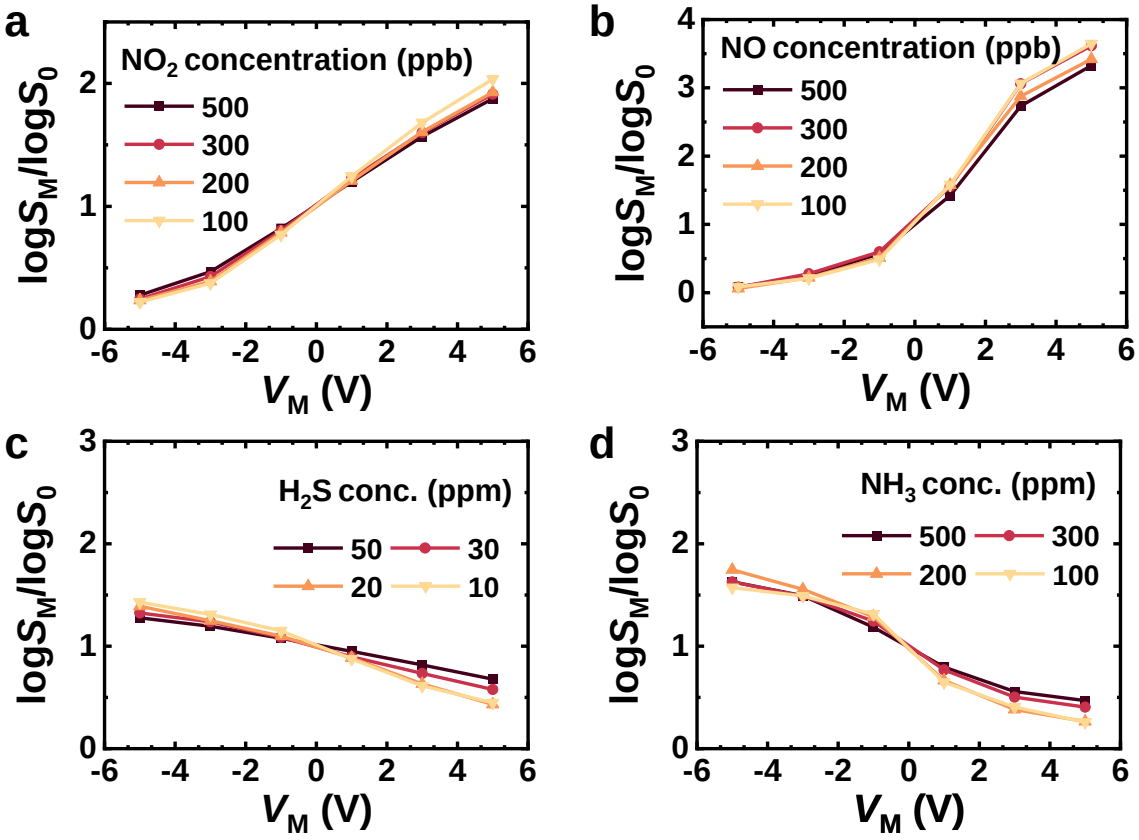

Supporting Fig. 13. logS_M/logS_0 vs. V_M curves of In_2O_3 sensor for varying concentrations of (a) NO_2, (b) NO, (c) H_2S, and (d) NH_3 gases.

Supporting Table 1 Adsorption energy (E_{ads}) of NO_2 gas on 18 sites of In_2O_3 (111) surface.

Site	e-rich	Pristine	e-deficient
A	-0.617	-0.149	-0.098
B	-0.895	-0.953	-0.130
C	-0.244	-0.078	-0.168
D	-1.388	-1.436	-0.556
E	-0.515	-0.129	-0.194
F	-1.388	-1.436	-0.556
G	-0.646	-0.151	-0.033
H	-0.331	-0.138	-0.217
I	-1.388	-1.436	-0.556
J	-0.657	-0.244	-0.207
K	-0.837	-0.850	-0.048
L	-1.387	-1.435	-0.556
M	-0.674	-0.217	-0.078
N	-0.764	-0.341	-0.230
O	-0.483	-0.084	-0.138
P	-0.458	-0.193	-0.022
Q	-0.833	-0.845	-0.127
R	-1.390	-1.437	-0.328

Supporting Note 1

To investigate the effect of V_M modulation on the carrier concentration of the adsorbent, we additionally fabricated devices with various channel lengths (L) (Figure S2a). We then measured the resistance of these devices while varying the V_M (Figure S2b). The obtained resistance can be expressed as follows:

$$R_{total} = R_{contact} + \rho \frac{L}{tW}$$

where, $R_{contact}$, ρ, t, and W represent the contact resistance, resistivity, thickness, and width, respectively. The resistivity of the adsorbent at various V_M values can be obtained from the slopes of the graphs shown in Figure S2b. The resistivity can be expressed as

$$\rho = \frac{1}{en\mu}$$

where e, n, μ represent the electron charge, electron density, and mobility. As shown in Figure S2c, which presents the electron density extracted from the above equation, the carrier concentration of the adsorbent can be controlled by adjusting the V_M.

Supporting Note 2

Most commercially available resistive gas sensors are not designed to control the carrier concentration in the adsorbent through the voltage applied to the heater terminal. However, in certain sensors, the heater and adsorbent are coupled, allowing for a slight adjustment in carrier concentration of adsorbent by applying voltage to the heater. The TGS-2602 sensor (Figaro Corp.) allows the carrier concentration of the adsorbent to be slightly adjusted by the heater terminal.